RESTORATION OF INTENSITY AND DEPTH IMAGES CONSTRUCTED USING SPARSE SINGLE-PHOTON DATA

Abderrahim Halimi, Yoann Altmann, Aongus McCarthy, Ximing Ren,
Rachael Tobin, Gerald S. Buller, Steve McLaughlin

School of Engineering and Physical Sciences, Heriot-Watt University, Edinburgh U.K.

ABSTRACT

This paper presents a new algorithm for the joint restoration of depth and intensity images constructed from the time-correlated single-photon counting (TCSPC) measurement in the limit of very few photon counts [1]. Under some justified approximations, the restoration problem (regularized likelihood) reduces to a convex formulation with respect to the parameters of interest. The first advantage of this formulation is that it only processes the corrupted depth and intensity images obtained from preliminary estimation, without the need for the use of full TCSPC waveforms. The second advantage is its flexibility in being able to use different convex regularization terms such as: total variation (TV); and sparsity of the discrete cosine transform (DCT) coefficients. The estimation problems are efficiently solved using the alternating direction method of multipliers (ADMM) that presents good convergence properties and thus a reduced computational cost. Results on single photon depth data from field trials show the benefit of the proposed strategy that improves the quality of the estimated depth and intensity images.

Index Terms— Lidar waveform, Poisson statistics, image restoration, ADMM, total variation regularization.

1. INTRODUCTION

Reconstruction of 3-dimensional scenes is a challenging problem encountered in many applications. For a given pixel, the time-of-flight laser detection and ranging (Lidar) system achieves this goal by emitting laser pulses and recording the reflected signal [2]. Single-photon Lidar typically uses a high repetition rate pulsed laser source in conjunction with a single-photon detector. The single-photon approach is used for its shot-noise limited sensitivity, and the temporal response means that the surface-to-surface resolution can be of millimeter scale. In single-photon Lidar, the recorded photon event is stored in a timing histogram which is constructed over a number of laser pulses. The time delay and the amplitude of the histogram are related to the distance and reflectivity of the observed object, respectively, which allows the construction of the 3D scene. In this paper, we consider the case when the acquisition time or the laser source power are small relative to the range of the target, which leads to a reduction in the number of detected photons per pixel. This problem can be solved by improving the instrument components [3, 4] or by taking a much longer time to acquire image data, which is rarely suitable. To most efficiently use the available sparse photon data, the alternative approach is to improve the processing of the acquired signals using signal processing techniques [5–7]. The latter approach will be considered here to improve the estimated depth and intensity (DI) images.

The first contribution of this paper is a new convex formulation for the cost function with respect to (w.r.t.) the DI images. Using the Poisson distribution of the observed photon counts, and introducing some justified approximations lead to a separable convex problem w.r.t. the parameters of interest. The obtained formulation is expressed w.r.t. preliminary estimates of the DI images which avoids the use of cumbersome photon count histograms during the refinement process. The resulting formulation can also be interpreted as an inpainting problem, which is efficiently solved using well known regularization terms such as total variation (TV) or the sparseness of the discrete cosine transform (DCT) coefficients.

The second contribution of this paper is the derivation of an estimation algorithm associated with the proposed cost functions. The alternating direction method of multipliers (ADMM) is used to solve the resulting problems by dividing them into simpler sub-problems. More precisely, the ADMM variant proposed in [8, 9] has been adapted to solve the proposed formulations. The proposed algorithms are fast (since they require simple operations) and show good convergence properties.

The paper is organized as follows. Section 2 introduces the observation model associated with the photon counts. The proposed formulation for DI restoration and the estimation algorithms are presented in Sections 3 and 4. Simulation results conducted using data acquired by an actual time-of-flight scanning sensor are presented and discussed in Section 5. Finally, conclusions and future work are reported in Section 6.

This work was supported by the EPSRC Grants EP/JO15180/1, EP/N003446/1, and EP/K015338/1

978-0-9928-6265-7/16/$31.00 ©2016 IEEE

2. OBSERVATION MODEL

The Lidar observation $\boldsymbol{y}_{i,j,t}$, where $(i,j) \in \{1,\cdots,N_r\} \times \{1,\cdots,N_c\}$, represents the number of photon counts within the tth bin of the pixel (i,j). According to [6, 10], each photon count $\boldsymbol{y}_{i,j,t}$ is assumed to be drawn from the Poisson distribution $\mathcal{P}(.)$ as follows

$$y_{i,j,t} \sim \mathcal{P}\left(s_{i,j,t}\right) \tag{1}$$

where

$$s_{i,j,t} = r_{i,j} g_0\left(t - t_{i,j}\right) + b_{i,j} \tag{2}$$

and $t_{i,j} \geq 0$ is the position of an object surface at a given range from the sensor (related to the depth), $r_{i,j} \geq 0$ is the intensity of the target, $b_{i,j} \geq 0$ is a constant denoting the background and dark photon level, and g_0 denotes the system impulse response assumed to be known from the calibration step. Assuming independence between the observed pixels leads to the joint likelihood

$$P(\boldsymbol{Y}|\boldsymbol{t},\boldsymbol{r},\boldsymbol{b}) = \prod_{i,j}\prod_{t=1}^{T} \frac{s_{i,j,t}^{y_{i,j,t}}}{y_{i,j,t}!} \exp^{-s_{i,j,t}} \tag{3}$$

where $\boldsymbol{t},\boldsymbol{r},\boldsymbol{b}$ are $N \times 1$ vectors gathering the elements $t_{i,j}$, $r_{i,j}$, $b_{i,j}, \forall i, \forall j$ (in lexicographic order), with $N = N_r N_c$, and T is the total number of bins.

3. PROBLEM FORMULATION

3.1. Estimation of the depth and intensity images

Using the Lidar waveforms $[\boldsymbol{Y}]_{i,j,t} = y_{i,j,t}$, the depth and intensity images of a given target are obtained by estimating $t_{i,j}$ and $r_{i,j}$, respectively. This goal can be achieved by maximizing the likelihood (3) w.r.t. $t_{i,j}, r_{i,j}, b_{i,j}$, or equivalently by minimizing the negative log-likelihood given by (after removing unnecessary constants)

$$\mathcal{L} = -\log\left[P(\boldsymbol{Y}|\boldsymbol{t},\boldsymbol{r},\boldsymbol{b})\right] = \sum_{i,j} \mathcal{L}_{i,j} + cst \tag{4}$$

where

$$\mathcal{L}_{i,j} = \sum_{t=1}^{T} \left[s_{i,j,t} - y_{i,j,t} \log\left(s_{i,j,t}\right)\right]. \tag{5}$$

To simplify the obtained cost function (5), the classical estimation approach (see [6] for more details) assumes the absence of the background level, i.e., $b_{i,j} = 0$. In this paper, we adopt this simplification and (in addition) assume a Gaussian approximation for the instrument impulse response $g_0\left(t - t_{i,j}\right) = c_1 \exp^{-\frac{\left(t-t_{i,j}\right)^2}{2\sigma^2}}$ as in [11], and that $c_2 = \sum_{t=1}^{T} g_0\left(t - t_{i,j}\right)$ is a constant for all realistic $t_{i,j}$ (which is justified since $T = 18000$ bins in Section 5 is higher than $\sigma \approx 5$ bins and the Gaussian is generally located in the center of the interval $[0,T]$). Under these assumptions, the cost function reduces to (after removing unnecessary constants)

$$\mathcal{L}_{i,j} = r_{i,j} - r_{i,j}^{\text{ML}} \left[\log\left(r_{i,j}\right) - \frac{\left(t_{i,j} - t_{i,j}^{\text{ML}}\right)^2}{2\sigma^2}\right] + i_{\mathbb{R}_+}\left(r_{i,j}, t_{i,j}\right) \tag{6}$$

where $i_{\mathbb{R}_+}(x,y)$ means $x \geq 0$ and $y \geq 0$, $t_{i,j}^{\text{ML}} = \frac{\left(\sum_{t=1}^{T} t y_{i,j,t}\right)}{\left(\sum_{t=1}^{T} y_{i,j,t}\right)}$ and $r_{i,j}^{\text{ML}} = \frac{1}{c_2}\left(\sum_{t=1}^{T} y_{i,j,t}\right)$ are the maximum of the simplified likelihood with respect to $t_{i,j}$ and $r_{i,j}$. The cost function, (6), obtained is interesting for two reasons. First, it does not include the Lidar observation terms $y_{i,j,t}$ explicitly, which means that our formulation considers only the two images $r_{i,j}^{\text{ML}}$ and $t_{i,j}^{\text{ML}}$ instead of the $N_r \times N_c \times T$ matrix $y_{i,j,t}$. Second, it is a sum of convex functions w.r.t. $t_{i,j}$ and $r_{i,j}$. Note finally that, due to the considered assumptions, the estimates $t_{i,j}^{\text{ML}}$ and $r_{i,j}^{\text{ML}}$ are of poor quality especially in the limit of very low photon counts. The next section introduces the regularization used to improve the estimated images from (6).

3.2. Image restoration

The quality of the depth and intensity images depends on two factors. The first is the acquisition time per pixel that needs to be high enough to provide an acceptable number of detected photons. However, this may lead to a long acquisition time which is not suitable for real applications (such as moving targets). The second is due to the assumptions used to estimate the images. Considerable effort is now devoted to reduce the acquisition and processing time of these images while keeping a good image quality. From a Bayesian perspective, this goal can be achieved by adding a priori knowledge about the images of interest to the likelihood (6). From an optimization perspective, the prior knowledge is equivalent to an additional regularization term $\phi(\boldsymbol{t},\boldsymbol{r})$ as described in the following sections.

3.2.1. Inpainting

A reduced number of photon counts is captured by the sensor when using a very low acquisition time. Under these conditions, many pixels might be empty ($\sum_{t=1}^{T} y_{i,j,t} = 0, \forall t$) leading to some pixels where DI estimation is impossible without additional information. This can be interpreted as an image inpainting problem that is accounted for by considering the following cost function

$$\mathcal{C}(\boldsymbol{t},\boldsymbol{r}) = \mathcal{L}(\boldsymbol{K}\boldsymbol{t},\boldsymbol{K}\boldsymbol{r}) + \phi(\boldsymbol{t},\boldsymbol{r}) \tag{7}$$

where K is an $Q \times N$ binary matrix that contains a single non-zero value on each line to model the loss of some image pixels and Q is the number of non-empty pixels. Due to its particular structure, this matrix satisfies $\boldsymbol{K}\boldsymbol{K}^T = \mathbb{I}_Q$, where $\mathbb{I}_Q$ is the $Q \times Q$ identity matrix.

3.2.2. Regularization

This paper studies two regularization terms to improve the image estimates. The first is the total variation (TV) regularization that assumes spatially correlated pixels (a four neighborhood structure is considered in this paper). This prior is

of great interest in the image processing community since it allows for noise reduction while preserving the edges. The cost function is given by

$$\mathcal{C}_{\text{TV}}(\boldsymbol{t},\boldsymbol{r}) = \mathcal{L}(\boldsymbol{K}\boldsymbol{t},\boldsymbol{K}\boldsymbol{r}) + \tau_1 \text{TV}(\boldsymbol{t}) + \tau_2 \text{TV}(\boldsymbol{r}) \quad (8)$$

where τ_1, τ_2 are the regularization parameters and $\text{TV}(\boldsymbol{x}) = \sum_{n=1}^{N} \sqrt{(\Delta_n^h \boldsymbol{x})^2 + (\Delta_n^v \boldsymbol{x})^2}$, where Δ_n^h and Δ_n^v are the horizontal and vertical first order differences at pixel n. The second regularization assumes the sparseness of the vectors $\boldsymbol{Dt}$ and $\boldsymbol{Dr}$, where $\boldsymbol{D}$ represents the discrete cosine transform (DCT) or contains in its column a wavelet basis. In this paper, we consider the sparseness of the DCT coefficients, i.e.,

$$\mathcal{C}_{\text{DCT}}(\boldsymbol{t},\boldsymbol{r}) = \mathcal{L}(\boldsymbol{K}\boldsymbol{t},\boldsymbol{K}\boldsymbol{r}) + \tau_3||\boldsymbol{D}\boldsymbol{t}||_1 + \tau_4||\boldsymbol{D}\boldsymbol{r}||_1 \quad (9)$$

where τ_3, τ_4 are the regularization parameters, D is the $N \times N$ matrix achieving the 2 dimensions-DCT transformation and $||.||_1$ is the sparsity imposing ℓ_1 norm.

4. ESTIMATION ALGORITHM

This section introduces the ADMM algorithms used to minimize (8) and (9). The first section introduces a general formulation of a variant of the ADMM algorithm. The later sections adapt this algorithm to the studied optimization problems.

4.1. General formulation

Consider the optimization problem $_J$

$$\underset{\boldsymbol{z}}{\text{argmin}}\, \mathcal{C}(\boldsymbol{z}) = \underset{\boldsymbol{z}}{\text{argmin}} \sum_{j=1} g_j\left(\boldsymbol{H}^{(j)}\boldsymbol{z}\right) \quad (10)$$

where $\boldsymbol{z} \in \mathbb{R}^d$, $g_j : \mathbb{R}^{p_j} \to \mathbb{R}$ are closed, proper, convex functions, and $\boldsymbol{H}^{(j)} \in \mathbb{R}^{p_j \times d}$ are arbitrary matrices. After denoting $\boldsymbol{u}^{(j)} = \boldsymbol{H}^{(j)}\boldsymbol{z} \in \mathbb{R}^{p_j}$ and introducing the auxiliary variable $\boldsymbol{d}^{(j)} \in \mathbb{R}^{p_j}$, the authors in [8] introduced the ADMM variant summarized in Algo. 1 to solve (10). This algorithm converges when the matrix $\boldsymbol{M} = \left[\sum_{j=1}^{J}\left(\boldsymbol{H}^{(j)}\right)^\top \boldsymbol{H}^{(j)}\right]$ has full rank, and the optimization problems in line 10 are solved exactly or if their sequences of errors are absolutely summable [8].

4.2. Restoration with TV regularization

Considering the $2N \times 1$ vector $\boldsymbol{z} = [\boldsymbol{t}^T, \boldsymbol{r}^T]^T = [\boldsymbol{z}_1^T, \boldsymbol{z}_2^T]^T$, the cost function (8) can be written as in (10) with

$$\begin{aligned}
g_1\left(u_i^{(1)}\right) &= u_i^{(1)} - r_i^{\text{ML}} \log\left(u_i^{(1)}\right), & \boldsymbol{H}^{(1)} &= [\boldsymbol{0}_N, \boldsymbol{K}] \\
g_2\left(u_i^{(2)}\right) &= \frac{\left(u_i^{(2)} - t_i^{\text{ML}}\right)^2}{2\frac{\sigma^2}{r_i^{\text{ML}}}}, & \boldsymbol{H}^{(2)} &= [\boldsymbol{K}, \boldsymbol{0}_N] \\
g_3\left(\boldsymbol{u}^{(3)}\right) &= \tau_1 \text{TV}(\boldsymbol{z}_1) + \tau_2 \text{TV}(\boldsymbol{z}_2), & \boldsymbol{H}^{(3)} &= \mathbb{I}_{2N} \\
g_4\left(\boldsymbol{u}^{(4)}\right) &= i_{\mathbb{R}_+^N}\left(\boldsymbol{u}^{(4)}\right), & \boldsymbol{H}^{(4)} &= [\mathbb{I}_N, \boldsymbol{0}_N]
\end{aligned} \quad (11)$$

Algorithm 1 ADMM variant for (10)

1: Initialization
2: Initialize $\boldsymbol{u}_0^{(j)}, \boldsymbol{d}_0^{(j)}, \forall j, \mu$. Set $k \leftarrow 0$, conv$\leftarrow 0$
3: **while** conv$= 0$ **do**
4: **for** j=1:J **do**
5: $\xi_k^{(j)} \leftarrow \boldsymbol{u}_k^{(j)} + \boldsymbol{d}_k^{(j)}$,
6: **end for**
7: $\boldsymbol{z}_{k+1} \leftarrow \boldsymbol{M}^{-1} \sum_{j=1}^{J}\left(\boldsymbol{H}^{(j)}\right)^\top \xi_k^{(j)}$,
8: **for** j=1:J **do**
9: $\boldsymbol{v}_k^{(j)} \leftarrow \boldsymbol{H}^{(j)}\boldsymbol{z}_{k+1} - \boldsymbol{d}_k^{(j)}$,
10: $\boldsymbol{u}_{k+1}^{(j)} \leftarrow \underset{\boldsymbol{s}}{\text{argmin}}\, \frac{\mu}{2}||\boldsymbol{s} - \boldsymbol{v}_k^{(j)}||^2 + g_j(\boldsymbol{s})$,
11: **end for**
12: **for** j=1:J **do**
13: $\boldsymbol{d}_{k+1}^{(j)} \leftarrow \boldsymbol{d}_k^{(j)} - \left(\boldsymbol{H}^{(j)}\boldsymbol{z}_{k+1} - \boldsymbol{u}_{k+1}^{(j)}\right)$,
14: **end for**
15: $k = k + 1$
16: **end while**

where $\boldsymbol{u}^{(3)} = \boldsymbol{z}$ and $\boldsymbol{M}$ reduces to a full rank diagonal matrix (fast to inverse). The optimization problems in line (10) are straightforward for $j = 1, 2$ and 3 and lead to exact solutions. As suggested in [8, 9], the TV problem in line (10) is solved using the iterative Chambolles algorithm [12]. This algorithm gives a sequence of errors absolutely summable (as empirically shown in [8,9]) which ensures the convergence of the ADMM algorithm. The resulting algorithm is denoted by RDI-TV for restoration of DI images using TV.

4.3. Restoration with DCT regularization

Similarly, the cost function (9) can be written as in (10) with the same g_1, g_2, g_4 and $\boldsymbol{H}^{(1)}, \boldsymbol{H}^{(2)}, \boldsymbol{H}^{(4)}$ as in (11). However, we have $g_3\left(\boldsymbol{u}^{(3)}\right) = \tau_3||\boldsymbol{z}_1||_1 + \tau_4||\boldsymbol{z}_2||_1$, $\boldsymbol{H}^{(3)} = \begin{bmatrix} \boldsymbol{D} & \boldsymbol{0}_N \\ \boldsymbol{0}_N & \boldsymbol{D} \end{bmatrix}$, Using $\boldsymbol{D}^T\boldsymbol{D} = \mathbb{I}_N$, leads to the same diagonal expression for $\boldsymbol{M}$ as in Section 4.2, which is easily invertible. The optimization problems in line (10) are straightforward and lead to exact solutions, which ensure the convergence of the proposed RDI-DCT algorithm. Note finally that the proposed RDI algorithms differ from [4, 6, 7] by considering a different cost function (a simplified convex formulation) and estimation algorithm (based on the ADMM).

5. SIMULATION RESULTS

This section evaluates the performance of the proposed restoration algorithms when considering six real images (142×142 pixels) of a life-sized polystyrene head, acquired at a distance of 40m. The images were acquired in November 2014 on the Edinburgh Campus of Heriot-Watt University, using a time-of-flight scanning sensor, based on TCSPC. The

Table 1. Processing time (in seconds).

	Acquisition time per pixel (ms)					
	0.06	0.3	0.6	3	6	30
RDI-TV	50	25	74	14	7	4
RDI-DCT	**7**	**8**	**8**	**5**	**4**	**1**
MCMC	6780	7380	7860	9120	11820	20820

transceiver system and data acquisition hardware used for this work are broadly similar to that described in [3, 5] (see also [6] for more details regarding the system parameters). The images considered have different acquisition time per pixel, i.e., 30ms, 6ms, 3ms, 600μs, 300μs and 60μs, where a long acquisition time leads to a better image quality. The proposed RDI algorithms are compared with the classical approach, and the MCMC based algorithm (both described in [6]) and with the BM3D algorithm [13]. The RDI algorithms require the regularization parameters to be set. In this study, we provide the best performance (in terms of RSNR) of these algorithms when testing three values centered around the following interval $(\tau_1, \tau_2, \tau_3, \tau_4) = (0.0025/c_2, 0.22, 0.001/c_2, 0.22)$ (we tested the doubles and the halves of these values). The restoration quality was evaluated using the reconstruction signal-to-noise ratio, $\text{RSNR} = 10\log_{10}\left(\frac{||\boldsymbol{x}||^2}{||\boldsymbol{x}-\widehat{\boldsymbol{x}}||^2}\right)$, where $\boldsymbol{x}$ is the reference depth or intensity image estimated with the classical approach for 30ms, $\widehat{\boldsymbol{x}}$ is the restored image and $||\boldsymbol{x}||^2$ denotes the ℓ_2 norm given by $\boldsymbol{x}^T\boldsymbol{x}$. Table 2 shows the obtained RSNR with the considered algorithms. The proposed RDI algorithms outperform the classical approach (in all cases) and the BM3D especially for the depth images and intensity images with high acquisition time. Images with many missing pixels (low acquisition time) are better processed by RDI-TV than RDI-DCT, while the latter shows good results for images with an acquisition time $\geq$ 3ms. Overall, the MCMC approach provides good performance, however, this is achieved at a price of a higher processing time, as highlighted in Table 1. Note that BM3D provides poor results for the depth images, however, it shows good performance for the intensity images with low acquisition time. Finally, Figs. 1 and 2 show examples of the obtained depth and intensity images with the different algorithms for the 0.3ms image. The MCMC algorithm generally presents the best visual results while RDI-TV and RDI-DCT clearly improve the performance of the classical approach.

6. CONCLUSIONS

This paper has presented a simplified formulation and a new algorithm for the joint restoration of depth and intensity images in the limit of very low photon counts. The proposed formulation reduced to a sum of convex functions suitable for the convergence of optimization techniques. The restoration of the two images (including the reconstruction of the missing pixels) was achieved by considering two regularization terms, the TV and the sparseness of the DCT coefficients. The resulting problems were solved using ADMM that has good convergence properties. The proposed formulation and algorithms showed good performance when processing real images in terms of the quality of the restored images and the computational cost. Future work includes the study of a joint regularization term for the depth and intensity images and the estimation of the RDI regularization parameters. Generalizing the algorithm to under-water images (where range-dependent signal attenuation occurs) is also an interesting issue which is worthy of investigation.

7. REFERENCES

[1] G. S. Buller and A. Wallace, "Ranging and three-dimensional imaging using time-correlated single-photon counting and point-by-point acquisition," vol. 13, no. 4, pp. 1006–1015, July 2007.

[2] M.-C. Amann, T. M. Bosch, M. Lescure, R. A. Myllylae, and M. Rioux, "Laser ranging: a critical review of unusual techniques for distance measurement," *Opt. Eng.*, vol. 40, pp. 10–19, Jan. 2001.

[3] A. McCarthy, X. Ren, A. D. Frera, N. R. Gemmell, N. J. Krichel, C. Scarcella, A. Ruggeri, A. Tosi, and G. S. Buller, "Kilometer-range depth imaging at 1550 nm wavelength using an InGaAs/InP single-photon avalanche diode detector," *Opt. Express*, vol. 21, no. 19, pp. 22 098–22 113, Sep 2013.

[4] A. Kirmani, D. Venkatraman, D. Shin, A. Colaço, F. N. C. Wong, J. H. Shapiro, and V. K. Goyal, "First-photon imaging," *Science*, vol. 343, no. 6166, pp. 58–61, 2014.

[5] A. M. Wallace, J. Ye, N. Krichel, A. McCarthy, R. Collins, and G. S. Buller, "Full waveform analysis for long-range 3d imaging laser radar," *EURASIP Journal on Advances in Signal Processing*, vol. 2010, no. 1, p. 896708, Dec. 2010.

[6] Y. Altmann, X. Ren, A. McCarthy, G. S. Buller, and S. McLaughlin, "Lidar waveform based analysis of depth images constructed using sparse single photon data," *IEEE Trans. Image Process.*, 2015, to appear.

[7] D. Shin, A. Kirmani, V. Goyal, and J. Shapiro, "Computational 3D and reflectivity imaging with high photon efficiency," in *Proc. IEEE Int. Conf. Image Process. (ICIP)*, Oct 2014, pp. 46–50.

[8] M. Figueiredo and J. Bioucas-Dias, "Restoration of poissonian images using alternating direction optimization," *IEEE Trans. Image Process.*, vol. 19, no. 12, pp. 3133–3145, Dec 2010.

[9] M. Afonso, J. Bioucas-Dias, and M. Figueiredo, "An augmented lagrangian approach to the constrained optimization formulation of imaging inverse problems," *IEEE Trans. Image Process.*, vol. 20, no. 3, pp. 681–695, March 2011.

[10] S. Hernandez-Marin, A. Wallace, and G. Gibson, "Bayesian analysis of lidar signals with multiple returns," *IEEE Trans. Pattern Anal. Mach. Intell.*, vol. 29, no. 12, pp. 2170–2180, Dec. 2007.

[11] Y. Altmann, A. Wallace, and S. McLaughlin, "Spectral unmixing of multispectral lidar signals," *IEEE Trans. Signal Process.*, vol. 63, no. 20, pp. 5525–5534, Oct 2015.

[12] A. Chambolle, "An algorithm for total variation minimization and applications," *J. Math. Imag. Vision*, vol. 20, no. 1, pp. 89–97, Jan. 2004.

[13] K. Dabov, A. Foi, V. Katkovnik, and K. Egiazarian, "Image denoising by sparse 3-d transform-domain collaborative filtering," *IEEE Trans. Image Process.*, vol. 16, no. 8, pp. 2080–2095, Aug 2007.

Table 2. RSNR (in dB) of the restored depth and intensity images w.r.t. the acquisition time.

		Acquisition time per pixel (ms)					
		0.06	0.3	0.6	3	6	30
Depth images	Class	3.36	11.93	18.56	37.13	38.42	-
	BM3D	3.72	14.72	24.79	37.11	37.43	38.01
	RDI-TV	**30.54**	**35.25**	36.23	**38.72**	39.09	70.24
	RDI-DCT	27.74	32.06	34.31	38.57	**39.50**	**82.50**
	MCMC	23.48	34.75	**37.13**	38.09	38.40	42.75
Intensity images	Class	0.01	5.19	7.01	9.44	10.66	-
	BM3D	**8.03**	**9.36**	9.12	9.40	9.31	9.51
	RDI-TV	2.0	9.05	**10.0**	**11.32**	**12.17**	14.94
	RDI-DCT	1.41	8.45	9.56	11.17	12.09	17.54
	MCMC	7.04	8.70	9.26	10.03	10.98	**34.72**

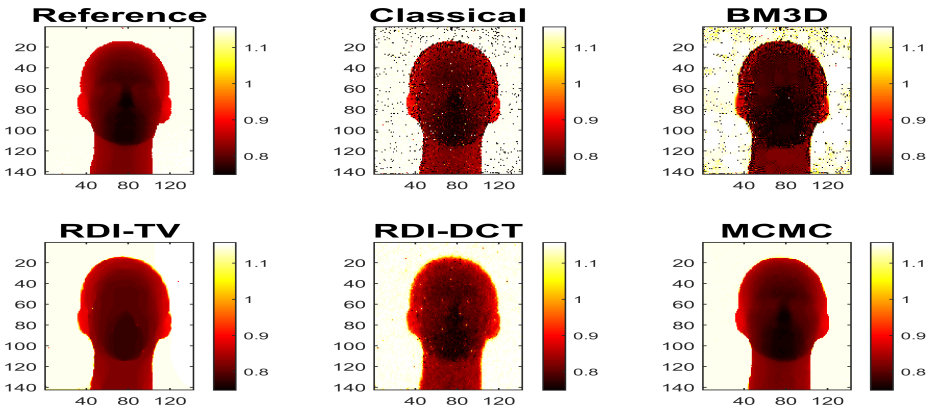

Fig. 1. Depth maps (142×142 pixels) of a life-sized polystyrene head produced using the 0.3ms per pixel image in conjunction with the algorithms considered. (top-left) reference depth, (top-middle) classical approach, (top-right) BM3D, (bottom-left) proposed RDI-TV, (bottom-middle) proposed RDI-DCT, and (bottom-right) MCMC approach [6].

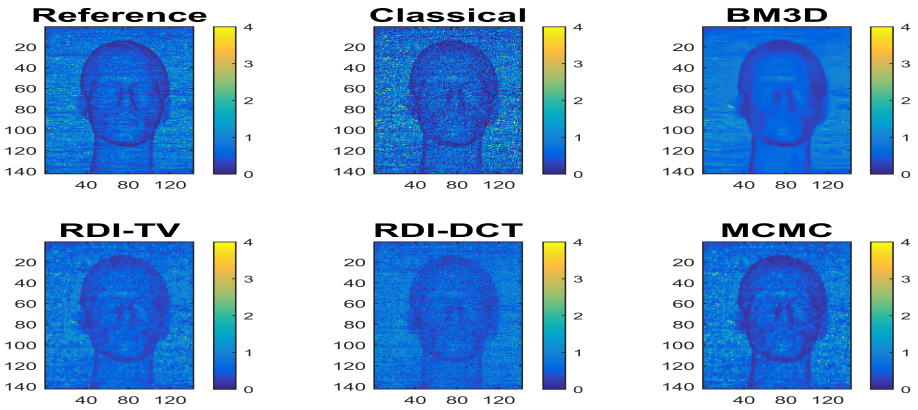

Fig. 2. Intensity maps (142×142 pixels) of a life-sized polystyrene head produced using the 0.3ms per pixel image in conjunction with the algorithms considered. (top-left) reference depth, (top-middle) classical approach, (top-right) BM3D, (bottom-left) proposed RDI-TV, (bottom-middle) proposed RDI-DCT, and (bottom-right) MCMC approach [6].